Structure in differential cross sections for electron-impact ionization of $Li^+(1s^2)$ in the coplanar equal-energy-sharing geometry

Xiang-Fu Jia*

Department of Physics, Shanxi Teachers University, Linfen, Shanxi 041004, People's Republic of China

(Received 27 August 2002; revised manuscript received 21 October 2002; published 26 December 2002)

The triple-differential cross section for electron-impact ionization of a $Li^+(1s^2)$ ion is considered in the coplanar equal-energy-sharing kinematics at an incident energy of 135.6 eV. The emergence of structures in the calculated cross sections is explained in terms of isolated two-body final-state interactions and three-body coupling. The cross section shows two peaks originating from ''classical'' sequential two-body collisions. The position of these peaks is determined by two-body final-state interactions. In addition, it is demonstrated that the signature of three-body interactions is carried by the magnitude and ratio of these two peaks. The direct and exchange amplitudes are also considered.

DOI: 10.1103/PhysRevA.66.062708 PACS number(s): 34.80.Dp, 34.80.Gs

I. INTRODUCTION

The understanding of the collision process involving ions is particularly important as atomic ions are bound in very hot environments such as fusion or astrophysical plasmas. Unfortunately, they are not present under normal conditions on the surface of the Earth. Thus it is with considerable difficulty that they can be produced in sufficient quantities for laboratory experiments. Theory is therefore of particular importance in this case for the following two reasons: to provide accurate data for cases where the experiments have not been done and to provide the framework for interpolation (or extrapolation) of the relevant data that exists.

Experiments for the ionization of ionic targets are limited to the total ionization and single-differential cross-section measurements [1–4]. Müller *et al.* [3], in their refined experiment (error $\sim 0.01\%$), have studied correlated two-electron transitions in the electron-impact ionization of a Li^+ ion, and were able to observe the resonant and nonresonant double excitation leading to single ionization. They noted that interference by resonance and direct ionization channels leads to a considerable enhancement of resonant features in the single-differential and total ionization cross section. Marrs *et al.* [5] have achieved the production of stationary hydrogenlike bare uranium ions, along with the measurements of the electron-impact ionization cross section. The ionization cross sections of Si^{4+} and Si^{5+} ions have been measured by Thompson and Gregory [6], and because of the absence of theoretical data they had to compare their cross section with that calculated using the semiclassical Lotz formula [7]. The shape of the cross-section curve is in agreement with that obtained using the Lotz formula, but the magnitude of the measured cross section is $\approx 20\%$ above the predictions of the calculations. Bray [8] proposed the convergent close-coupling approximation for studying the electron-impact ionization of ions and calculated the total ionization cross sections for He^+ and O^+ ions. Their results are in good agreement with the experimental results of Perth *et al.* [9] and Defrance *et al.* [10].

Theoretical as well as experimental works regarding the $(e,2e)$ triple-differential cross sections (TDCS) for ionic targets are scanty. The additional difficulty that arises in studying the electron-impact ionization of an ionic target, as compared to the neutral one, is the presence of a long-range Coulomb interaction. Roy, Roy, and Sil [11], in their calculation of $(e,2e)$ triple-differential ionization cross sections for the He^+ ion, did not include the electron-electron correlation in the final channel, and as a result their final-state wave function does not satisfy the proper three-body boundary conditions. Biswas and Sinha [12] suggested a model in which the scattered (faster) outgoing electron is treated in the framework of the eikonal approximation, while the ejected (slower) electron is represented by a Coulomb wave. The correlation between the two outgoing electrons is taken into account through the eikonal phase term and Coulomb parameters. In an earlier paper [13] we extended the Brauner-Briggs-Klar (BBK) model [14] for hydrogen and helium ions, in which the incident electron is described by a Coulomb wave in the presence of a screened ionic nucleus, and the final channel is represented by the BBK wave function. The basic difference between the Biswas and Sinha [12] approach and our approach [13] lies in the choice of the prescription for the final-channel wave function. The final-state wave function is chosen as the three-body Coulomb continuum [14], which satisfies the proper three-body asymptotic boundary condition. The prescription of the final is superior in the sense that the former is mainly appropriate for asymmetric geometric only, while the latter is suitable for both the symmetric and asymmetric geometries and hence is more versatile.

The BBK model [14] should be regarded as a significant advance in the theory of $(e,2e)$ processes, in which a three-Coulomb (3C) product wave function was first used to describe the final state. This 3C wave function was quite successful in reproducing the TDCS for electron-impact ionization of hydrogen [14] and helium [15] at high and intermediate energies. However, for low incident energies, the calculated TDCS using the BBK wave function are not in agreement with experiment [16]. The major limitation of the BBK model lies in the fact that the dynamic screening of any two-body Coulomb interaction, i.e., the influence on the strength of the interaction of any two particles by the pres-

*Email address: jiaxf@dns.sxtu.edu.cn

ence of the third one, has not been taken into account. This deficiency was first corrected by Berakdar and Briggs [16] through the introduction of new Sommerfeld parameters for the symmetric case in which the two outgoing electrons have equal energies (therefore we refer to this model as DS3C). Chen *et al*. [17] have extended the work of Berakdar and Briggs by both symmetric and asymmetric cases and the results turned out to be in quite good agreement with the measurements [17–19].

The TDCS caused by electron-impact ionization depends on the geometry as well as kinematics, and therefore, a proper understanding of their roles is essential for explaining the collision dynamics. An investigation of electron-impact ionization of ionic targets would therefore be quite useful and interesting. Therefore, the present work investigates mainly the ionization of Li^+ using the DS3C model suggested by Berakdar and Briggs [16]. The TDCS for ionization has been determined in the coplanar equal-energy-sharing kinematics at an incident energy of 135.6 eV. As our aim is to explain the physical processes underlying structures observed in the TDCS, only the major features of the theory used are briefly summarized in Sec. II. In Sec. III we concentrate on the interpretation of the angular pattern of the TDCS and in Sec. IV conclusions are drawn. Atomic units (a.u.) are used unless otherwise specified.

II. THEORETICAL MODEL

In this section we briefly sketch the theoretical model. Here we consider a $Li^+(1s^2)$ target being single ionized by the impact of an electron with incident momentum $\mathbf{k}_i$. The spin-nonresolved TDCS for the coincident detection of two continuum electrons escaping with momenta $\mathbf{k}_a$ and $\mathbf{k}_b$ and emerging into direction defined by solid angles Ω_a and Ω_b is given by

$$\frac{d^3\sigma}{d\Omega_a d\Omega_b d(k_b^2/2)} = (2\pi)^4 \frac{k_a k_b}{k_i}\left[\tfrac{3}{4}|f(\mathbf{k}_a,\mathbf{k}_b)-g(\mathbf{k}_a,\mathbf{k}_b)|^2 + \tfrac{1}{4}|f(\mathbf{k}_a,\mathbf{k}_b)+g(\mathbf{k}_a,\mathbf{k}_b)|^2\right], \quad (1)$$

where $f(\mathbf{k}_a,\mathbf{k}_b)$ and $g(\mathbf{k}_a,\mathbf{k}_b)$ are the direct and exchange amplitudes, respectively, with $f(\mathbf{k}_b,\mathbf{k}_a)=g(\mathbf{k}_a,\mathbf{k}_b)$. The direct amplitude is

$$f(\mathbf{k}_a,\mathbf{k}_b)=\langle \Psi_f^-(\mathbf{r}_a,\mathbf{r}_b,\mathbf{r}_c)|V_i|\Psi_i^+(\mathbf{r}_a,\mathbf{r}_b,\mathbf{r}_c)\rangle, \quad (2)$$

where $\mathbf{r}_a,\mathbf{r}_b,\mathbf{r}_c$ denote the position vectors of the incoming electron "a" and the two bound electrons "b" and "c," respectively, with respect to the nucleus.

The initial channel wave function Ψ_i^+ in Eq. (2) is chosen in the framework of the Coulomb-Born approximation as

$$\Psi_i^+(\mathbf{r}_a,\mathbf{r}_b,\mathbf{r}_c)=F_c(\mathbf{k}_i,\mathbf{r}_a)\phi_i(\mathbf{r}_b,\mathbf{r}_c), \quad (3)$$

where F_c represents a Coulomb wave function due to the long-range Coulomb attraction between the incident electron and the screened target ion and is given by

$$F_c(\mathbf{k}_i,\mathbf{r}_a)=(2\pi)^{-3/2}e^{\pi\alpha_i/2}\Gamma(1+i\alpha_i) \times e^{i\mathbf{k}_i\cdot\mathbf{r}_a}\,{}_1F_1(i\alpha_i;1;i(k_i r_a-\mathbf{k}_i\cdot\mathbf{r}_a)) \quad (4)$$

with $\alpha_i=1/k_i$. ${}_1F_1(a;b;c)$ is the confluent hypergeometric function. The ground-state wave function of the $Li^+(1s^2)$ $\phi_i(\mathbf{r}_b,\mathbf{r}_c)$ in Eq. (3) is chosen as the simple Hylleraas form

$$\phi_i(\mathbf{r}_b,\mathbf{r}_c)=u(\mathbf{r}_b)u(\mathbf{r}_c), \qquad u(r)=\left(\frac{\lambda^3}{\pi}\right)^{1/2}e^{-\lambda r}, \quad (5)$$

with $\lambda=(Z_t-1)+0.6875$. Z_t is the charge of the heliumlike target ion.

Perturbation corresponding to this initial state is given by

$$V_i=V_{ee}+V_{en}+V_{ec}=\frac{1}{r_{ab}}-\frac{(Z_t-1)}{r_a}+\frac{1}{r_{ac}}, \quad (6)$$

with $r_{ab}=|\mathbf{r}_a-\mathbf{r}_b|$, $r_{ac}=|\mathbf{r}_a-\mathbf{r}_c|$. Hence, Eq. (2) may be rewritten as

$$f=T_{ee}+T_{en}+T_{ec}=\langle\Psi_f^-|V_{ee}|\Psi_i^+\rangle+\langle\Psi_f^-|V_{en}|\Psi_i^+\rangle + \langle\Psi_f^-|V_{ec}|\Psi_i^+\rangle. \quad (7)$$

Here T_{ee}, T_{en}, and T_{ec} represent T-matrix elements in which the initial scattering is off the active (ionized) electron, nucleus, and passive electron, respectively. Hence the sum $T_{en}+T_{ec}=T_{core}$ represents the initial scattering of the incident electron off the Li^{2+} core.

In order to construct the wave function Ψ_f^- for the final channel, which involves four particles, the following assumptions have been adopted. We have reduced the four-body problem to a three-body one in the sense that the bound passive electron plays no other role than to screen the nucleus from the two outgoing particles. The final-channel correlated wave function Ψ_f^- is given by

$$\Psi_f^-(\mathbf{r}_a,\mathbf{r}_b,\mathbf{r}_c)=(2\pi)^{-3/2}e^{\pi\alpha_a/2}\Gamma(1+i\alpha_a)e^{i\mathbf{k}_a\cdot\mathbf{r}_a} \times {}_1F_1(-i\alpha_a;1;-i(k_a r_a+\mathbf{k}_a\cdot\mathbf{r}_a)) \times e^{\pi\alpha_{ab}/2}\Gamma(1+i\alpha_{ab}) \times {}_1F_1(-i\alpha_{ab};1;-i(k_{ab}r_{ab}+\mathbf{k}_{ab}\cdot\mathbf{r}_{ab})) \times\phi(r_b,r_c), \quad (8)$$

where $\mathbf{k}_{ab}=(\mathbf{k}_a-\mathbf{k}_b)/2$, and

$$\phi(\mathbf{r}_b,\mathbf{r}_c)=[\bar{\phi}_{\mathbf{k}_b}(\mathbf{r}_b)\phi_f(\mathbf{r}_c)+\bar{\phi}_{\mathbf{k}_b}(\mathbf{r}_c)\phi_f(\mathbf{r}_b)]/\sqrt{2}, \quad (9)$$

$$\bar{\phi}_{\mathbf{k}_b}(\mathbf{r})=\phi_{\mathbf{k}_b}(\mathbf{r})-\langle\phi_{\mathbf{k}_b}|u\rangle u(r). \quad (10)$$

The wave function $\phi(\mathbf{r}_b,\mathbf{r}_c)$ of the two-electron ion (Li^+) subsystem in the final channel has been represented by a symmetrized product of the one-electron (Li^{2+}) ground-state wave function (ϕ_f) for the bound electron ($\mathbf{r}_c$) with the continuous wave function $\bar{\phi}_{\mathbf{k}_b}$ for the ejected electron with momentum $\mathbf{k}_b$ [orthogonalized to the ground-state orbital $u(r)$].

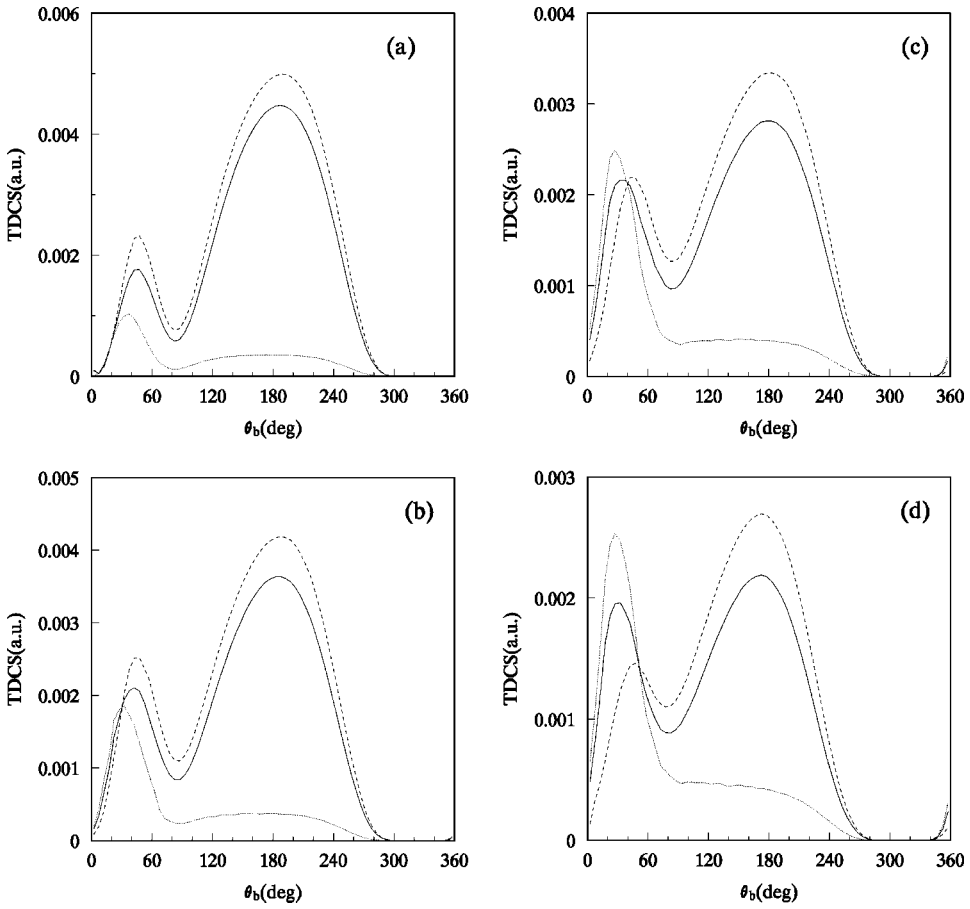

FIG. 1. The TDCS in atomic units (a.u.) for the ionization of $Li^+(1s^2)$ by electron impact in the coplanar equal-energy-sharing kinematics at incident energy $E_i = 135.6$ eV, $E_a = E_b = 30$ eV, as a function of ejected electron angle θ_b. The scattering angle θ_a is fixed to (a) $\theta_a = 20°$, (b) $\theta_a = 30°$, (c) $\theta_a = 40°$, and (d) $\theta_a = 50°$. The solid curve represents the present results, the broken curve and dotted one correspond to the calculations of the direct $f(\mathbf{k}_a, \mathbf{k}_b)$ and the exchange $g(\mathbf{k}_a, \mathbf{k}_b)$ amplitudes, respectively.

It should be noted here that in calculating the matrix element corresponding to the second term (i.e., the exchange term) in Eq. (9), we have also replaced the coordinates b and c in the remaining part of the expression of $\Psi_f^-(\mathbf{r}_a, \mathbf{r}_b, \mathbf{r}_c)$ in Eq. (8) for the sake of consistency.

The ejected electron is described by the following screened Coulomb wave function:

$$\phi_{k_b}(\mathbf{r}) = (2\pi)^{-3/2} e^{\pi\alpha_b/2} \Gamma(1 + i\alpha_b) e^{i\mathbf{k}_b \cdot \mathbf{r}_b} \times {}_1F_1(-i\alpha_b; 1; -i(k_b r_b + \mathbf{k}_b \cdot \mathbf{r}_b)). \quad (11)$$

In Eqs. (8) and (11) α_i $[i \in (a,b,ab)]$ are Sommerfeld parameters. The assumption that the three-body system consists of three spatially independent two-body systems leads to the representation of the Sommerfeld parameters in the BBK model [14] as $\alpha_a = 2/k_a$, $\alpha_b = 2/k_b$, and $\alpha_{ab} = -1/2k_{ab}$.

However, the Sommerfeld parameter is a measure of the strength of the Coulomb interaction between charged particles, and the strength of the interaction of any two particles in the three-body Coulomb system is affected by the presence of the third one. Having recognized this, Berakdar and Briggs suggested [16] the DS3C model to modify the 3C wave function by formulating the effective Sommerfeld parameters. Here we cite the explicit functional form for the case of equal energy sharing ($\mathbf{k}_a = \mathbf{k}_b = \mathbf{k}$) as

$$\alpha_a = \alpha_b = \frac{4Z_{eff} - \sin\theta}{4k}, \quad \alpha_{ab} = \frac{-1 + \sin^2\theta}{2k \sin\theta}, \quad (12)$$

where the angle θ is defined as $\theta = (\cos^{-1}\hat{\mathbf{k}}_a \cdot \hat{\mathbf{k}}_b)/2$, and effective charge Z_{eff} of the $Li^{2+}(1s)$ core seen by the escaping electrons is taken as [20]

$$Z_{eff} = (Z_t - 1) + 0.5052 e^{-2.5496 E_i}. \quad (13)$$

The ionization amplitude as described in Eq. (1) finally involves a three-dimensional integration, which has been evaluated numerically. For numerical integrations we have adopted a technique similar to that of our previous work [13] with necessary modifications.

III. RESULTS AND DISCUSSIONS

We have computed the TDCS for electron-impact ionization of the $Li^+(1s^2)$ ion at 135.6 eV incident electron energy. The coplanar equal-energy-sharing geometry has been studied by taking account of electron exchange in the final channel. The results have been displayed in Figs. 1(a)–1(d), where the present TDCS have been plotted against the angle of ejection (θ_b) of the ejected electron and the deflected projectile electron is detected at fixed angles of $\theta_a = 20°, 30°, 40°, 50°$, respectively. Since no TDCS measurements have yet been performed for the ionic species, we are not in a position to compare our results with experiments.

In all cases we notice a double-peak structure in the angular distributions. Before we proceed with analyzing the dynamical origin of these structures, it is advantageous to study the classical kinematical properties of the collisions

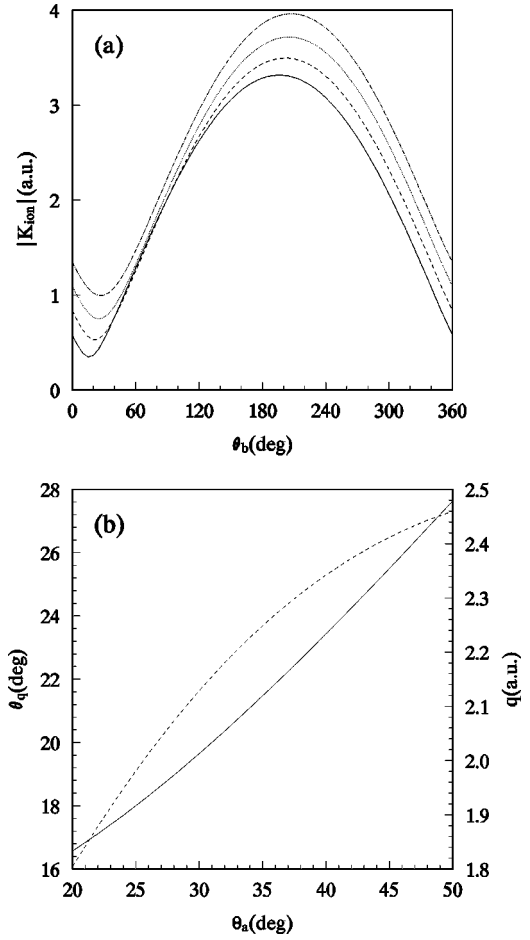

FIG. 2. (a) The recoil-ion momentum $\mathbf{k}_{ion}$ as a function of the emission angle (θ_b). The full, broken, dotted, and chain curves refer to the cases where $\theta_a = 20°$, 30°, 40°, and 50°, respectively. (b) The magnitude q (solid curve) and the angle θ_q (dashed curve) of the momentum transfer are depicted as a function of the scattering angle θ_a in the range investigated here.

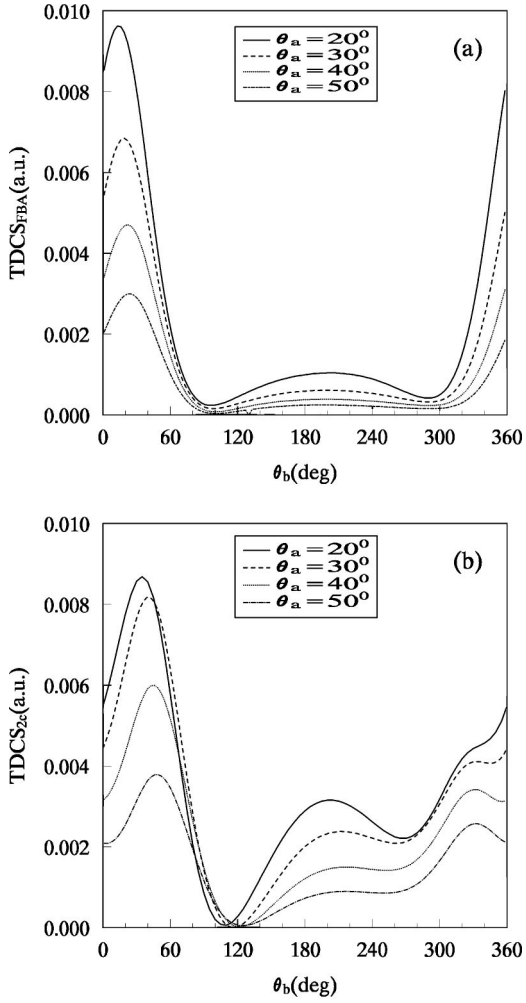

FIG. 3. The same collision geometry as in Figs. 1(a)–1(d) studied in the approximations (a) the first Born approximation (FBA) and (b) the independent Coulomb particle model (2C). The curves (full, broken, dotted, and chain) correspond to different fixed scattering angles ($\theta_a = 20°$, 30°, 40°, and 50°, respectively).

that are common to all dynamical models. Investigating the spectrum of the recoil-ion momentum can elucidate this. We note that as a consequence of the translational invariance of the reaction the linear momentum is conserved during the collision, i.e., $\mathbf{k}_{ion}(\theta_b) = \mathbf{k}_i - \mathbf{k}_a - \mathbf{k}_b$, where $\mathbf{k}_{ion}(\theta_b)$ is the recoil momentum of $Li^{2+}(1s)$, which is assumed to be initially at rest. As seen in Fig. 2(a), the angular behavior of the recoil-ion momentum can be directly linked to the momentum transferred to the target during the collision, which we define as $\mathbf{q} = \mathbf{k}_i - \mathbf{k}_a$. If the ejected electron is emitted along $\hat{\mathbf{q}}$, the momentum transferred to the target is mainly absorbed by the secondary electron and little momentum is transferred to the $Li^{2+}(1s)$ (only via initial-state binding). Thus a minimum occurs in $\mathbf{k}_{ion}(\theta_b)$ at $\theta_b = \theta_q = \cos^{-1}(\hat{\mathbf{k}}_i \cdot \hat{\mathbf{q}})$. This is seen nicely by comparing Figs. 2(a) and 2(b). With increasing scattering angle θ_a of the projectile electron the momentum-transfer direction $\hat{\mathbf{q}}$ moves away from the incident direction [cf. Fig. 2(b)]. The position of the minimum in $\mathbf{k}_{ion}(\theta_b)$ exactly follows this behavior. Besides, with increasing θ_a the magnitude of the momentum transferred to the target ion is increased as a evident from Fig. 2(b). Thus the overall magnitude of $\mathbf{k}_{ion}$ is enhanced with increasing θ_a. As evident from Figs. 2(a) and 2(b), the broad peak in $\mathbf{k}_{ion}(\theta_b)$ is located in the direction where the ionized electrons emerge opposite to the direction $\mathbf{q}$, i.e., at $\theta_b = \theta_q + 180°$. The link between the structure of $\mathbf{k}_{ion}(\theta_b)$ and $\mathbf{q}$ supports the identification of the minima and maxima appearing in Fig. 2(a) as being the results of certain (sequential) two-body classical collisions. In the single-binary region, where $\mathbf{k}_b \| \mathbf{q}$, the two electrons collide almost independently of the $Li^{2+}(1s)$ ion and hence there is a minimum momentum transferred to it. $Li^{2+}(1s)$ is a spectator to the electron-electron collision. Classically the momentum transfer to $Li^{2+}(1s)$ vanishes in this case, provided the initial-momentum distribution of the ionic electron is neglected. The peak appearing in $\mathbf{k}_{ion}(\theta_b)$ at the recoil region, i.e., at $(\hat{\mathbf{k}}_b \cdot \hat{\mathbf{q}}) = -1$, can be assigned to double-binary collisions where the secondary electron scatters off the nucleus after a binary encounter with the projectile. The broadness of the peaks and minima of $\mathbf{k}_{ion}(\theta_b)$ is

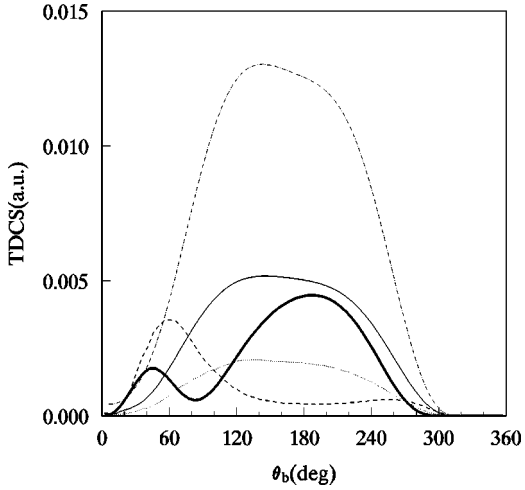

FIG. 4. The same geometry as in Fig. 1(a). The incoherent contributions to the TDCS (solid thick curve) of the scattering amplitudes T_{ee} (broken curve), T_{en} (dash-dot curve), T_{ec} (dotted curve), and the coherent sum (between T_{en} and T_{ec}) T_{core} (light solid curve).

due to the initial-momentum distribution of the three-body system. This broadening is more pronounced the lower the impact energy and tends to flatten the structure in $\mathbf{k}_{ion}(\theta_b)$. Nevertheless, it has been shown by Berakdar and Briggs [21] that for the electron-impact ionization of atomic hydrogen, even at excess energies as low as 2 eV, the behavior of $\mathbf{k}_{ion}(\theta_b)$ as described above can still be seen.

The information on $\mathbf{k}_{ion}(\theta_b)$ can also be linked to the structure of the spin unresolved cross section, as shown in Figs. 1(a)–1(d). Here we observe the emergence of two peaks at positions near the binary and recoil emission directions as discussed above. However, only the positions of these peaks can be traced to the structure of $\mathbf{k}_{ion}(\theta_b)$ and thus to the collision-ionization mechanisms outlined above. This is evident by comparing results of different dynamical models: DS3C [cf. Figs. 1(a)–1(d)], first Born approximation (FBA) [in Eq. (8) $\alpha_a=\alpha_{ab}=0$] and independent Coulomb particle model (2C) [in Eq. (8) $\alpha_{ab}=0$] [cf. Figs. 3(a) and 3(b)] where the kinematics are the same. The shift of the positions of these peaks is readily understood by comparing Fig. 1 and Fig. 3. In the FBA model, where the ionized electron occupies a target-continuum state, the position of the peaks coincides with the positions of the classical binary and recoil peaks. The heights of the peaks decrease monotonically as q increases [cf. Fig. 3(a)]. In the FBA, the electrons, although of identical energy, are treated unequally. In the 2C model, in which the two continuum electrons move independently in the $Li^{2+}(1s)$ ion field, the binary peak is shifted away from the scattered electron direction, whereas the recoil peak appears nearer to $-\mathbf{q}$. The angular distribution predicted by the 2C cross section [cf. Fig. 3(b)] shows a new peak near $\theta_b>330°$, i.e., the two electrons emerge preferentially in nearly the same direction but well away from the position of maximum Li^{2+} recoil. Finally, including the electron-electron final-state interactions [Figs. 1(a)–1(d)] squeezes the angular distributions of the ejected electrons away from the direction of the scattering electron.

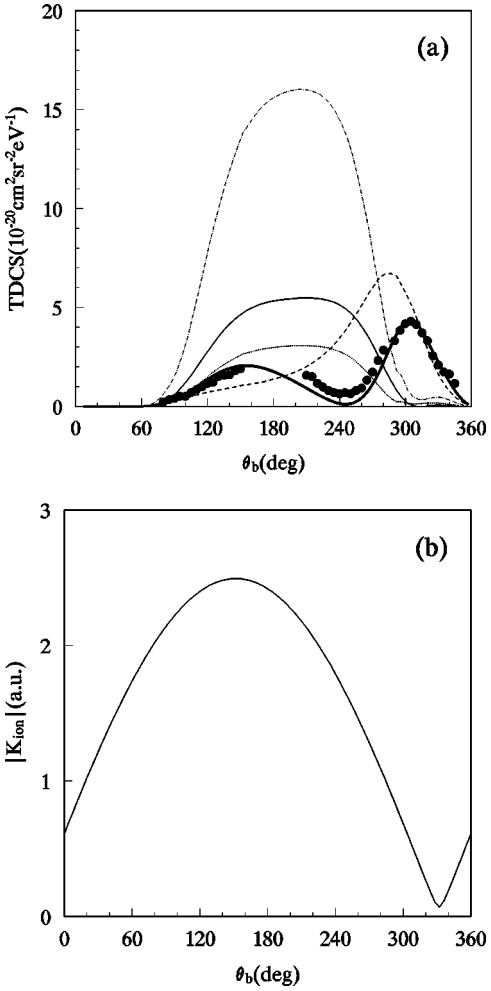

FIG. 5. (a) TDCS for electron-impact ionization of $He(1s^2)$ at incident energy $E_i=64.6$ eV in the coplanar equal-energy-sharing geometry for fixed angle of $\theta_a=-30°$. The circles are the experimental measurements of Bray *et al.* [22]. The solid thick curve is the present results, while the others are the same as Fig. 4. The present calculations have been multiplied by a factor of 0.66. (b) The angular distribution of the recoil-ion momentum in the case depicted in (a).

From the preceding discussion and by comparing the heights of the peaks in different dynamical models, it is obvious that the magnitudes of the peaks are a subtler feature than their positions. In fact, viewed in the present theory, the actual shape of the cross section is determined by three-body coupling, as the only difference between the approximations 3C and DS3C is the inclusion of three-body coupling in the latter one [16]. Three-body interactions control the interference pattern of various scattering amplitudes by differently weighting these amplitudes. This is evident from Fig. 4 where the magnitudes of the scattering amplitudes from the bound electron T_{ee} and the ion (Li^{2+}) T_{core} are examined separately. As expected, the major contribution to the cross section around the binary region comes from T_{ee}, whereas T_{core} (the coherent sum of the scattering amplitudes T_{en} and T_{ec}) dominates over T_{ee} in the recoil regions. Although experimental data do not exist for the ion target here, there are data that show the appearance of precisely such a structure.

In this case the data are for a helium target and the emerging electrons are measured at fixed angle $\theta_a = -30°$ and with energies $E_a = E_b = 20$ eV [cf. Fig. 5(a)]. The extension of the theory presented in the preceding section to a helium target can be obtained through $\alpha_i = 0$ and $Z_t = 2$. The results are shown in Fig. 5(a). The information concerning the mechanisms responsible for scattering into different angular regions can be gleaned from an examination of the recoil-ion momentum as a function of the scattering angle. The recoil-ion momentum spectrum is shown in Fig. 5(b) for helium. The curves show only two features: a minimum in the recoil-ion momentum when $\theta_b = 330°$, i.e., the electrons emitted symmetrically with respect to the beam direction (the single-binary configuration) and a broad maximum for the backward emission of both electrons. The peak of maximum occurs at $\theta_b = 152°$. This supports strongly the identification of the processes leading to ionization in the configuration. The cross section is calculated as a coherent sum of contributions of electron-electron (T_{ee}) and electron-ion (T_{core}) scattering. In Fig. 5(a) the separate (incoherent) contributions of electron-electron (T_{ee}) and electron-ion (T_{core}) scattering are also displayed. Incoherent scattering amplitudes can still be traced to two-body scattering processes. The observed cross sections, however, are determined by the interference pattern of these amplitudes, which is decided by three-body coupling. This theoretical study has been confirmed by further experimental data in a different kinematical arrangement [23].

Another point that warrants investigation is the effect of the indistinguishability of the escaping electrons. It is worthwhile to consider the exchange amplitude in the coplanar symmetric energy-sharing geometry. From Figs. 1(a)–1(d) it can be seen that around the binary region the TDCS are mainly contributed by the direct *f* and exchange *g* scattering amplitudes, whereas the direct amplitude *f* dominates over *g* in the recoil regions. The exchange effects become more important as θ_a increases. The effect of antisymmetrization on the final outcome for the spin-unresolved TDCS is important. Therefore, the indistinguishability of the two electrons plays a major role in determining the shape of the angular distribution.

IV. CONCLUSIONS

In this work the TDCS for the electron-impact ionization of $Li^+(1s^2)$ in the coplanar equal-energy sharing has been investigated at an excess energy of 60 eV. It has been shown that the cross section reveals a double-peak structure. The positions of these peaks are primarily determined by classical single- and double-binary collisions and are modified by final-state interactions. It is demonstrated that the relative height of the peaks is the signature of three-body coupling in a three-body Coulomb system. If the coupling is neglected, only a poor description results. In addition, the exchange effects have also been considered. We have shown the situation in which the exchange effects are crucial.

It is worth nothing that there have been several successful nonperturbative theories for electron-impact ionization of neutral atoms (see Refs. [24,25]). Good agreement has been found between theory and experiment. It would be very interesting to apply these theories to electron-impact ionization of ionic targets. As there are no other results available, we have to wait for them to test the reliability of the present results.

ACKNOWLEDGMENTS

This work was supported by the Natural Science Foundation of Shanxi Province (Grant No. 20001008) and the Science Foundation for Returnee of Shanxi Province [Grant No.(99)13] of China.

[1] K.T. Dolder and B. Peart, Rep. Prog. Phys. **39**, 693 (1976).
[2] S.M. Younger, Phys. Rev. A **26**, 3177 (1980).
[3] A. Müller, G. Hofmann, B. Weissbecker, M. Strenke, K. Tinschert, M. Wagner, and E. Salzborn, Phys. Rev. Lett. **63**, 758 (1989).
[4] D. Fang, W. Hu, J. Tang, Y. Wang, and F. Yang, Phys. Rev. A **47**, 1861 (1993).
[5] R.E. Marrs, S.R. Elliott, and D.A. Knapp, Phys. Rev. Lett. **72**, 4082 (1994).
[6] J.S. Thompson and D.C. Gregory, Phys. Rev. A **50**, 1377 (1994).
[7] W. Lotz, Z. Phys. **216**, 205 (1968).
[8] I. Bray, Aust. J. Phys. **49**, 201 (1996).
[9] B. Perth, D.S. Wolton, and K.T. Dolder, J. Phys. B **2**, 1347 (1969).
[10] P. Defrance, F. Brouillard, F. Claeys, and G. Wassenhov, J. Phys. B **14**, 103 (1981).
[11] A. Roy, K. Roy, and N.C. Sil, J. Phys. B **15**, 1289 (1982).
[12] R. Biswas and C. Sinha, J. Phys. B **28**, 1311 (1995).
[13] X.F. Jia, Q.C. Shi, Z.J. Chen, J. Chen, and K.Z. Xu, Phys. Rev. A **55**, 1971 (1997).
[14] M. Brauner, J.S. Briggs, and H. Klar, J. Phys. B **22**, 2265 (1989).
[15] M. Brauner, J.S. Briggs, and J.T. Broad, J. Phys. B **24**, 287 (1991).
[16] J. Berakdar and J.S. Briggs, Phys. Rev. Lett. **72**, 3799 (1994).
[17] Z.J. Chen, Q.C. Shi, S.M. Zhang, J. Chen, and K.Z. Xu, Phys. Rev. A **56**, R2514 (1997).
[18] Z.J. Chen, S.M. Zhang, Q.C. Shi, J. Chen, and K.Z. Xu, J. Phys. B **30**, 4963 (1997).
[19] Z.J. Chen and K.Z. Xu, Chin. Phys. **10**, 290 (2001).
[20] J. Berakdar and J.S. Briggs, J. Phys. B **27**, 4271 (1994).
[21] J. Berakdar and J.S. Briggs, J. Phys. B **29**, 2289 (1996).
[22] I. Bray, D.V. Fursa, J. Röder, and H. Ehrhardt, J. Phys. B **30**, L101 (1997).
[23] J. Berakdar, J.S. Briggs, I. Bray, and D.V. Fursa, J. Phys. B **32**, 895 (1999).
[24] I. Bray and D.V. Fursa, Phys. Rev. A **54**, 2991 (1996).
[25] M. Baertschy, T.N. Rescigno, W.A. Isaacs, X. Li, and C.W. McCurdy, Phys. Rev. A **63**, 022712 (2001).